A Point Mutation in the Pore Region Alters Gating, Ca^{2+} Blockage, and Permeation of Olfactory Cyclic Nucleotide–gated Channels

Paola Gavazzo,* Cristiana Picco,* Elisabeth Eismann,‡ U. Benjamin Kaupp,‡ and Anna Menini*§

From the *Istituto di Cibernetica e Biofisica, Consiglio Nazionale delle Ricerche, 16149 Genova, Italy; ‡Institut für Biologische Informationsverarbeitung, 52425 Jülich, Germany; and §Biophysics Sector, International School for Advanced Studies, 34014 Trieste, Italy

abstract Upon stimulation by odorants, Ca^{2+} and Na^+ enter the cilia of olfactory sensory neurons through channels directly gated by cAMP. Cyclic nucleotide–gated channels have been found in a variety of cells and extensively investigated in the past few years. Glutamate residues at position 363 of the α subunit of the bovine retinal rod channel have previously been shown to constitute a cation-binding site important for blockage by external divalent cations and to control single-channel properties. It has therefore been assumed, but not proven, that glutamate residues at the corresponding position of the other cyclic nucleotide–gated channels play a similar role. We studied the corresponding glutamate (E340) of the α subunit of the bovine olfactory channel to determine its role in channel gating and in permeation and blockage by Ca^{2+} and Mg^{2+}. E340 was mutated into either an aspartate, glycine, glutamine, or asparagine residue and properties of mutant channels expressed in *Xenopus laevis* oocytes were measured in excised patches. By single-channel recordings, we demonstrated that the open probabilities in the presence of cGMP or cAMP were decreased by the mutations, with a larger decrease observed on gating by cAMP. Moreover, we observed that the mutant E340N presented two conductance levels. We found that both external Ca^{2+} and Mg^{2+} powerfully blocked the current in wild-type and E340D mutants, whereas their blockage efficacy was drastically reduced when the glutamate charge was neutralized. The inward current carried by external Ca^{2+} relative to Na^+ was larger in the E340G mutant compared with wild-type channels. In conclusion, we have confirmed that the residue at position E340 of the bovine olfactory CNG channel is in the pore region, controls permeation and blockage by external Ca^{2+} and Mg^{2+}, and affects channel gating by cAMP more than by cGMP.

key words: cyclic guanosine monophosphate • cyclic adenosine monophosphate • olfactory sensory neurons • site-directed mutagenesis

INTRODUCTION

Olfactory transduction is initiated by the binding of odorant molecules to receptor proteins located in the cilia of olfactory sensory neurons. This binding causes the activation of a receptor-coupled G protein, which in turn activates an adenylyl cyclase that synthesizes cAMP. The resultant increase in cAMP concentration leads to the opening of cyclic nucleotide–gated (CNG)[1] ion channels in the ciliary membrane (Nakamura and Gold, 1987), through which flows an odorant-induced current carried by Na^+ and Ca^{2+} ions. Ca^{2+} entry in olfactory sensory neurons is physiologically important since a rise in intracellular Ca^{2+}concentration is involved both in the excitation process, which includes the activation of a Ca^{2+}-activated Cl^- current, and in adaptation (for a recent review, see Menini, 1999).

Native CNG channels from olfactory sensory neurons have been supposed to be heterotetrameric complexes with two types of subunits, named differently by different authors. However, a third type of subunit, a short splice variant of the retinal rod β subunit, has recently been cloned (Sautter et al., 1998) and CNG channels from rat olfactory sensory neurons have been shown to be comprised of three different types of subunits (Bönigk et al., 1999). Unfortunately, an agreement on the nomenclature for CNG channels has not yet been reached, creating confusion for the nonspecialist reading papers on CNG channels. We will use the nomenclature of Bönigk et al. (1999); i.e., α3 for the principal olfactory α subunit, α4 for the second cloned subunit (this subunit was originally named rOCNC2 by Bradley et al., 1994, and Liman and Buck, 1994, and subsequently named β subunit by other authors) and β1b for the most recently cloned subunit (Sautter et al., 1998; Bönigk et al., 1999). The α3 subunit expressed in *Xenopus laevis* oocytes forms functional channels (Dhallan et al., 1990; Altenhofen et al., 1991; Goulding et al., 1992), while the other two subunits, α4 and β1b, are modulatory subunits and do not form functional CNG channels on their own. The α3 subunit has a glutamate

Address correspondence to Dr. Anna Menini, Biophysics Sector, International School for Advanced Studies, Via Beirut 2, 34014 Trieste, Italy. Fax: 39-040-2240470; E-mail: menini@sissa.it

[1]*Abbreviation used in this paper:* CNG channel, cyclic nucleotide–gated channel.

residue (E340) that corresponds to E363 of the α subunit of the bovine rod CNG channel. The two subunits α4 and β1b have an aspartate and a glycine residue, respectively, at the corresponding location.

Each CNG channel subunit is formed by six transmembrane segments, with the pore region located between the fifth and sixth transmembrane segment (for reviews, see Kaupp, 1995; Menini, 1995; Zimmerman, 1995; Finn et al., 1996; Zagotta and Siegelbaum, 1996). Structure–function studies have identified several domains of the channel protein involved in channel gating: a cyclic nucleotide-binding domain, near the COOH terminus (Kaupp et al., 1989; Altenhofen et al., 1991; Brown et al., 1993; Scott and Tanaka, 1998), a region near the NH_2 terminus (Goulding et al., 1994; Gordon and Zagotta, 1995; Varnum et al., 1995; Tibbs et al., 1997), the C-linker, which connects the sixth transmembrane segment and the cyclic nucleotide-binding domain (Brown et al., 1998; Zong et al., 1998; Paoletti et al., 1999), and the pore (Bucossi et al., 1997; Fodor et al., 1997). The cyclic nucleotide–binding site is physically separated from the pore region and the mechanism by which the conformational change in the cyclic nucleotide–binding domain is coupled to channel opening is likely to be very complex, with several regions of the channel being involved (Sun et al., 1996; Gordon et al., 1997; Varnum and Zagotta, 1997; Becchetti et al., 1999; Sunderman and Zagotta, 1999a,b).

A number of previous studies have reported that extracellular Ca^{2+} effectively blocks the current carried by monovalent ions through retinal rod, cone, and olfactory CNG channels in a voltage-dependent way (for reviews, see Kaupp, 1995; Menini, 1995; Finn et al., 1996). Site-directed mutagenesis on the α subunit of CNG channels from bovine retinal rods showed that blockage by external Ca^{2+} and Mg^{2+} critically depends on E363 (Root and MacKinnon, 1993; Eismann et al., 1994). Retinal rod, cone, and olfactory CNG channels share many functional properties, but also differ in some respects. For example, cGMP and cAMP activate similar maximal currents in olfactory CNG channels, whereas cAMP activates only a small fraction of the current activated by cGMP in rod and cone CNG channels. Moreover, Ca^{2+} permeation is higher in CNG channels of olfactory sensory neurons and cones compared with rods (Perry and McNaughton, 1991; Frings et al., 1995; Picones and Korenbrot, 1995).

The aim of the present study was to investigate the role in permeation, gating, and block by Ca^{2+} and Mg^{2+} of the residue at position 340 in the α3 subunit of the bovine olfactory CNG channel.

MATERIALS AND METHODS

Site-directed Mutagenesis and Functional Expression

Site-directed mutagenesis was performed following the procedure of Herlitze and Koenen (1990). The cDNA of the bovine olfactory CNG channel (Altenhofen et al., 1991) was mutated by PCR reaction at the level of the putative pore region, where the sequence encoding the glutamate residue in position 340 was substituted with the sequence encoding a residue of aspartic acid or with the sequence encoding noncharged amino acids such as glutamine, asparagine, and glycine. Mutant clones were selected by their sensitivity to a nearby introduced SgrAI site and verified by sequencing (Sanger et al., 1977). mRNAs specific for the wild-type and mutant channels were then synthesized in vitro (Melton et al., 1984) from XhoI-linearized DNA using T3-RNA polymerase; synthesis was primed with m7G(5′)ppp(5′)G. *Xenopus laevis* oocytes (Centre National de la Recherche Scientifique, Montpellier, France) were prepared and injected with individual mRNAs as previously described (Gavazzo et al., 1997).

Current Recordings

Current measurements were performed from patches excised from the plasma membrane of oocytes in the inside-out or outside-out configuration.

Macroscopic currents were measured with the Axopatch 1D patch-clamp amplifier (Axon Instruments, Inc.), filtered at 1 kHz, and sampled at 2 or 2.5 kHz using a TL-1 DMA interface board (Axon Instruments, Inc.) with a PC-type computer and pClamp5 software (Axon Instruments, Inc.).

Single-channel recordings, performed 1–3 d after mRNA injection, allowed the determination of single-channel current and open probability of wild-type and mutant channels. Single-channel traces were recorded filtering at 2 kHz and sampled at 10 kHz. All-points amplitude histograms were constructed from 30 s of data recordings. The single-channel current and the open probability were determined by analyzing amplitude histograms normalized to a total area of 1. Histograms were fitted using the Levenberg-Marquardt least square algorithm by the sum of two or more Gaussian functions with pClamp6 software (Axon Instruments, Inc.).

Ionic Solutions

The ionic composition of the divalent cation-free solution at the extracellular and intracellular sides of the membrane patch was: 110 mM NaCl, no added divalent salts, 2 mM EDTA, and 10 mM HEPES, buffered to pH 7.4 with NaOH or with tetramethylammonium hydroxide. Low Ca^{2+} or Mg^{2+} concentrations were buffered by 2 mM nitrilotriacetic acid or by EDTA, respectively. The concentrations of $CaCl_2$ or $MgCl_2$, necessary to give the indicated free Ca^{2+} or Mg^{2+} concentrations were calculated using the chelator program of Fabiato (1988). Free Ca^{2+} or Mg^{2+} concentrations higher than 0.1 mM were not buffered.

Channels were activated with various concentrations of cyclic nucleotides, cGMP or cAMP, applied at the intracellular side of an excised patch. Exchange of bath solutions was achieved by positioning the excised patch in front of one of four glass pipes from which test solutions were continuously flowing, as previously described by Menini and Nunn (1990).

Current–Voltage Relations

Macroscopic current–voltage relations were measured by applying voltage steps of 150-ms duration from a holding potential of 0 mV in ±20-mV steps. For the measurement of the current blockage by divalent cations, current–voltage relations were obtained by ramping the voltage command from −80 to +80 mV in 1 s; five individual ramps were averaged in each measurement. I-V relations at the beginning of each experiment were also measured by applying voltage steps of 150-ms duration to investigate whether the patch presented ion accumulation effects, as de-

scribed by Zimmerman et al. (1988). The experiments were continued only when such effect was not present and therefore the I-V relations obtained from ramps or from voltage steps gave the same values.

Outside-out patches were used to investigate the blockage by external Ca^{2+} and Mg^{2+}. In these experiments, 1 mM cGMP was present in the patch pipette, unless otherwise indicated. Similar results were obtained when channels were activated by cAMP. The leak conductance was assumed not to be voltage dependent, and was usually estimated by perfusing the external side of the patch with a solution containing 73.3 mM $CdCl_2$ or $MgCl_2$ buffered to pH 7.4 with tetramethylammonium hydroxide. The residual conductance measured at negative potentials was taken as the leak conductance and was subtracted from each I-V relation. Further experiments were only performed when the leak current did not exceed 10% of the CNG current in divalent cation-free solution.

Data Analysis of Dose–Response Relations

Macroscopic currents as a function of cyclic nucleotide concentration were fitted by:

$$I = I_{max} c^n / (c^n + K^n{}_{1/2}), \quad (1)$$

where I is the activated current, I_{max} is the maximal current, c is the cyclic nucleotide concentration, $K_{1/2}$ is the cyclic nucleotide concentration activating half of the maximal current, and n is the Hill coefficient.

A similar equation was used to fit the single-channel open probability, P_o, as a function of cyclic nucleotide concentration:

$$P_o = P_{max} c^n / (c^n + K^n{}_{1/2}), \quad (2)$$

where P_{max} is the maximal open probability and $K_{1/2}$ is the cyclic nucleotide concentration giving the half-maximal open probability.

A model for channel activation involving the cooperative binding of cyclic nucleotides to n binding sites, followed by an allosteric closed to open transition, similar to that originally proposed by Liu et al. (1994), was also used (Scheme I):

$$C + cN \underset{K_1}{\rightleftharpoons} (C\text{-}cN) + cN \underset{K_2}{\rightleftharpoons} (C\text{-}cN_2) + cN \underset{K_3}{\rightleftharpoons} \cdots (C\text{-}cN_{n-1}) + cN \underset{K_n}{\rightleftharpoons} (C\text{-}cN_n) \underset{L}{\rightleftharpoons} O$$

(SCHEME I)

where C is the channel in the closed state, cN is the cyclic nucleotide, O is the channel in the open state, K_i are the dissociation constants for the binding sites, and L is the equilibrium "gating" constant, defined as the ratio between open and closed channels. In the limiting case of infinite cooperativity between the binding sites, the above kinetic scheme reduces to Scheme II:

$$C + n\,cN \underset{K_d}{\rightleftharpoons} (C\text{-}cN_n) \underset{L}{\rightleftharpoons} O \quad \text{(SCHEME II)}$$

with K_d representing the "effective" dissociation constant, defined as $K_d = (K_1 K_2 \cdots K_{n-1} K_n)^{1/n}$. In this model, the channel open probability, P_o, is given by:

$$P_o = [L/(1+L)][c^n / c^n + K^n{}_{1/2}], \quad (3)$$

where c is the cyclic nucleotide concentration and $K_{1/2} = K_d / (1+L)^{1/n}$. Therefore, $K_{1/2}$ values are determined by both the apparent ligand affinity for cyclic nucleotides and the probability of the allosteric transition. The maximal open probability, P_{max}, is given by $L/(1+L)$.

The parameters obtained by fitting the single-channel dose–response data to the Hill equation (P_{max}, $K_{1/2}$, and n) (Eq. 2) were used to calculate starting points for the parameters L, K_d, and n for the best fit of Eq. 3. Curve fittings were done with IgorPro3.1 (WaveMetrics).

Data Analysis of Current Blockage

Current values in the presence of various concentrations of Ca^{2+} or Mg^{2+} were normalized to the current in the absence of divalent cations at a given voltage and plotted versus divalent cation concentration. Data were fitted with the following equation:

$$I/I_{max} = 1 - [d^n / (d^n + K^n{}_i)], \quad (4)$$

where I is the current measured in the presence of the divalent cation concentration d, I_{max} is the current measured in the absence of divalent cations, K_i is the divalent cation concentration blocking half of I_{max}, and n is the Hill coefficient.

Eq. 4 was fitted to the data for each patch separately and mean values for K_i and n were calculated. All data are given as mean ± SD.

RESULTS

Macroscopic Currents

Currents activated by cGMP or cAMP were studied in excised inside-out patches from oocytes expressing wild-type or individual mutant channels. Fig. 1, A and B, shows macroscopic currents measured at voltage pulses between −80 and +80 mV and activated by cGMP (A) or by cAMP (B) concentrations producing maximal currents.

In wild-type channels, maximal currents activated by cGMP or cAMP have very similar values; whereas, quite surprisingly, we found that in the E340G mutant, the current activated by cAMP was reduced to ~50% of the current activated by cGMP. Mutation of E340 to aspartate, asparagine, or glutamine had much smaller effects on maximal currents activated by cAMP (see Table I).

In Fig. 1 C, the modification of the current–voltage relations induced by mutations of E340 is shown. The mean ratio between the cAMP-gated current flowing at −80 and +80 mV, $I(-80)/I(+80)$, was 1.12 ± 0.03 (n = 7) in wild-type channels, while it was slightly more inwardly rectifying in the mutated channel E340D, with a ratio of 1.30 ± 0.08 (n = 8) and became progressively outwardly rectifying with ratios of 0.69 ± 0.12 (n = 8) in the E340G, 0.51 ± 0.10 (n = 6) in the E340N, and 0.18 ± 0.05 (n = 5) in the E340Q mutants. Rectification ratios were similar for channels activated by cAMP or by cGMP (Table I). Whether changes of the current–voltage dependence were due to a modification of the channel permeation or gating properties caused by the mutations will be investigated later (see Fig. 4).

Normalized dose–response relations at −80 mV are shown in Fig. 1, D and E. Currents for each channel

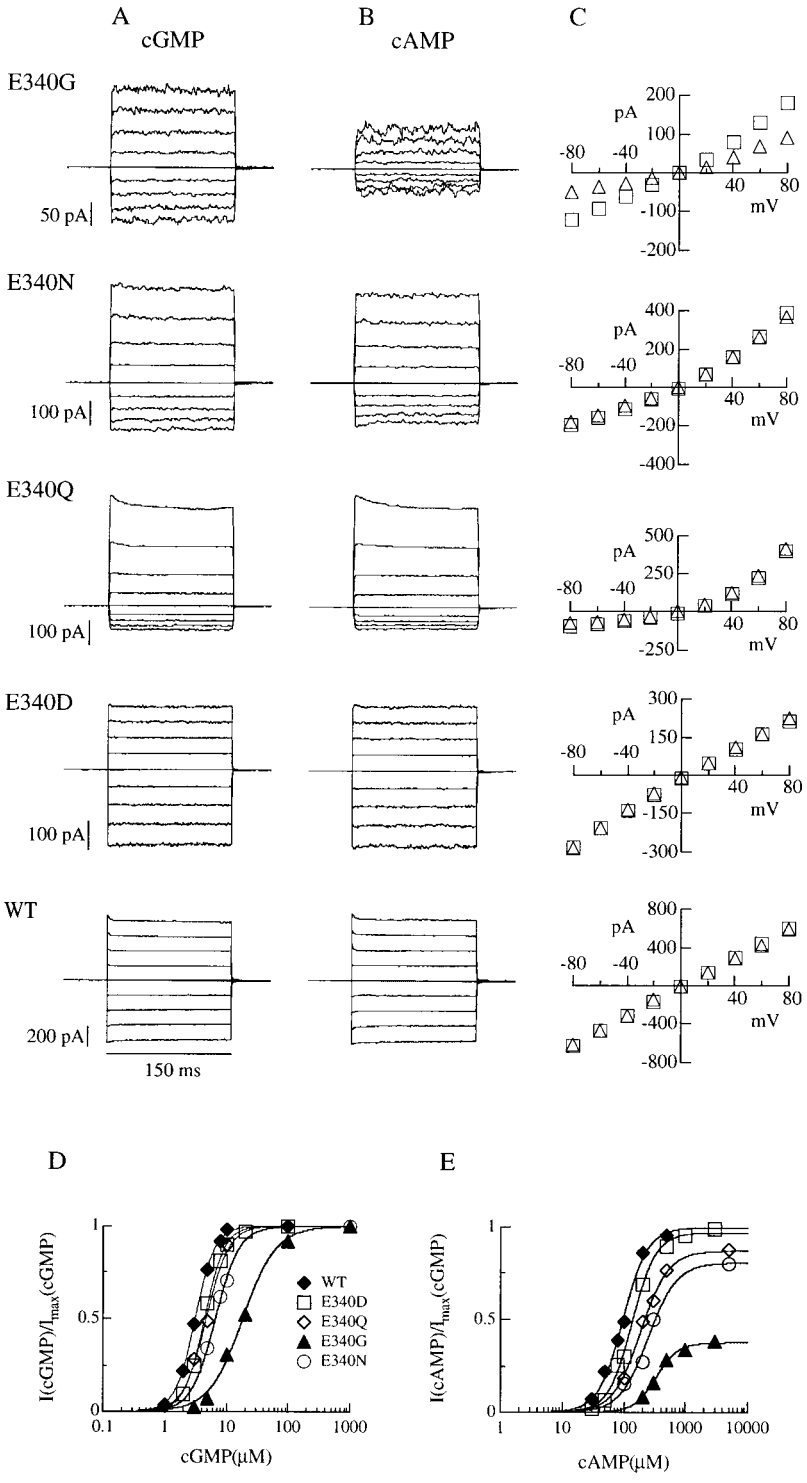

Figure 1. Maximal currents activated by cGMP or cAMP for wild-type and mutant olfactory CNG channels. Currents in each row were from the same excised inside-out patch. Voltage steps of 150-ms duration from a holding potential of 0 mV were given from −80 to +80 mV in 20-mV steps. Currents were activated by cyclic nucleotide concentrations eliciting maximal currents (see dose–response relations in D–E): (A) cGMP concentration was 1 mM, (B) cAMP concentration was 3 mM for E340G and E340D, 5 mM for E340N and E340Q, and 500 μM for wild-type channels. (C) Current–voltage relations from recordings shown in A and B for cGMP (□) and cAMP (△). (D–E) Dose–response relations. Currents activated by cGMP or by cAMP at −80 mV were measured in the same patch, normalized to the maximal current activated by cGMP at −80 mV, and plotted versus cGMP (D) or cAMP (E) concentrations. Continuous lines represent the best fit of the Hill equation (Eq. 1) to the data with the following values. Wild-type: $I_{max,cA}/I_{max,cG}$ = 0.99, $K_{1/2,cG}$ = 3.2 μM, n_{cG} = 2.7, $K_{1/2,cA}$ = 97 μM, n_{cA} = 2.2; E340D: $I_{max,cA}/I_{max,cG}$ = 0.97, $K_{1/2,cG}$ = 4.5 μM, n_{cG} = 2.7, $K_{1/2,cA}$ = 137 μM, n_{cA} = 2.3; E340Q: $I_{max,cA}/I_{max,cG}$ = 0.87, $K_{1/2,cG}$ = 4.8 μM, n_{cG} = 2.4, $K_{1/2,cA}$ = 189 μM, n_{cA} = 2.0; E340N: $I_{max,cA}/I_{max,cG}$ = 0.81, $K_{1/2,cG}$ = 6.6 μM, n_{cG} = 2.3, $K_{1/2,cA}$ = 251 μM, n_{cA} = 1.9; E340G: $I_{max,cA}/I_{max,cG}$ = 0.37, $K_{1/2,cG}$ = 18.5 μM, n_{cG} = 1.6, $K_{1/2,cA}$ = 335 μM, n_{cA} = 2.5.

type were measured from the same patch, plotted versus the concentration of cGMP or cAMP, fitted by the Hill equation (Eq. 1), and normalized to the maximal current measured in cGMP at −80 mV. For all mutants, the dose–response relations were shifted towards higher cyclic nucleotide concentrations with respect to the wild-type channel (Table I). At −80 mV, $K_{1/2}$ for cGMP increased from an average value of 2.5 ± 0.5 μM (n = 7) for the wild-type to 15.5 ± 1.6 μM (n = 3) for the E340G mutant, and $K_{1/2}$ for cAMP increased from an average value of 73 ± 19 μM (n = 7) for the wild-type to 430 ± 66 μM (n = 5) for the E340G mutant. Moreover, the maximal current of the E340G mutant activated by cAMP was 0.44 ± 0.05 (n = 8) of that acti-

TABLE I

Parameters of Dose–Response Relations from Macroscopic Currents from Mutant and Wild-Type CNG Channels

					$K_{1/2}$, μM					
	I(cAMP) / I(cGMP)		I(−80 mV) / I(+80 mV)		cAMP		cGMP		n(−80 mV)	
	−80 mV	+80 mV	cAMP	cGMP	−80 mV	+80 mV	−80 mV	+80 mV	cAMP	cGMP
Wild Type	0.98 ± 0.02	0.97 ± 0.20	1.12 ± 0.03	1.11 ± 0.03	73 ± 19	78 ± 21	2.5 ± 0.5	2.6 ± 0.6	2.3 ± 0.4	2.7 ± 0.2
	(7)	(7)	(7)	(7)	(7)	(7)	(7)	(7)	(7)	(7)
E340D	0.91 ± 0.09	0.93 ± 0.06	1.30 ± 0.08	1.30 ± 0.10	152 ± 20	155 ± 20	4.9 ± 1.1	4.8 ± 1.1	1.9 ± 0.2	2.6 ± 0.4
	(8)	(8)	(8)	(8)	(6)	(6)	(6)	(6)	(6)	(6)
E340G	0.44 ± 0.05	0.50 ± 0.06	0.69 ± 0.12	0.79 ± 0.09	430 ± 66	453 ± 37	15.0 ± 1.6	13.0 ± 1.5	2.0 ± 0.4	1.8 ± 0.4
	(8)	(8)	(8)	(8)	(5)	(5)	(3)	(3)	(5)	(3)
E340N	0.83 ± 0.07	0.91 ± 0.06	0.51 ± 0.10	0.55 ± 0.10	299 ± 31	206 ± 35	7.6 ± 4.0	5.6 ± 1.8	2.0 ± 0.3	2.1 ± 0.3
	(6)	(6)	(6)	(6)	(7)	(7)	(7)	(7)	(7)	(7)
E340Q	0.89 ± 0.05	0.96 ± 0.06	0.18 ± 0.05	0.19 ± 0.06	194 ± 83	141 ± 31	5.6 ± 1.7	4.0 ± 1.2	1.8 ± 0.4	2.7 ± 0.5
	(5)	(5)	(5)	(5)	(4)	(4)	(4)	(4)	(4)	(4)

Data are obtained by fitting the experimental values with the Hill equation (Eq. 1). All values are means ± SD, with the number of experiments in parenthesis.

vated by cGMP. Other mutations affected the current ratio less (Table I).

Therefore, mutations of glutamate 340 changed the voltage dependence of currents and modified the channel activation by increasing $K_{1/2}$ and decreasing the ratio between maximal currents activated by cAMP and cGMP.

Single-Channel Properties

To interpret properties of the macroscopic currents in terms of permeation and gating behavior, currents from patches containing only one single olfactory CNG channel were recorded.

Fig. 2, A and B, shows recordings at −80 mV from a patch containing a single E340G channel. The open probability was plotted in Fig. 2 C as a function of cyclic nucleotide concentrations and fitted by the Hill equation (Eq. 2). At −80 mV, the average $K_{1/2}$ was 14 ± 5 μM (n = 4) for cGMP and 400 ± 214 μM (n = 4) for cAMP. These values are very similar to those obtained from macroscopic dose–response relations (see Table I).

In the presence of cGMP, the average maximal open probability, P_{max}, for E340G channels was 0.79 ± 0.06 (n = 9), whereas, in the presence of cAMP, P_{max} was only 0.27 ± 0.12 (n = 9). These values were much lower than P_{max} for the wild-type channel, 0.996 ± 0.001 (n = 3) with cGMP and 0.985 ± 0.004 (n = 5) with cAMP (data not shown). The open probability was largely independent of voltage (see Table II).

Therefore, the maximal open probability measured in the E340G mutant was significantly lower than that of the wild-type channel and its value depended on which cyclic nucleotide activated the channel.

Single-channel properties were also investigated in other mutants. Single-channel currents from the mutant E340Q could not be measured, probably because of their small amplitude. Assuming the existence of only one open state, an estimate of the current amplitude was obtained by the relation between current variance and mean amplitude of macroscopic currents at various cGMP concentrations (data not shown). The estimated single-channel current was 0.1 pA at +80 mV and 0.03 pA at −80 mV, with a maximal open probability of 0.9.

Fig. 3 A shows recordings from a patch containing one single E340N mutant channel obtained at two cGMP concentrations at +80 and −80 mV.

Two conductance levels were present. The low conductance state had a current amplitude of ∼1 pA at +80 mV. From the low conductance state, the channel made brief transitions to a higher conductance state of ∼2.5 pA. Occasionally, the current trace returned to baseline from the low conductance state. Transitions to the high conductance state were never observed from the baseline, but only from the low conductance state. At a low cGMP concentration (3 μM), the channel spent most of the time in the closed state, from which it opened to the low conductance state, and very rarely to the high conductance state, as shown in the amplitude histogram of Fig. 3 B. At a high cGMP concentration (100 μM), the channel spent most of the time in the low conductance state from which it made more frequent but brief transitions to the high conductance state (Fig. 3 C).

The low conductance state was outwardly rectifying [i = −0.5 ± 0.1 pA (n = 5) at −80 mV, and 1.0 ± 0.2 pA (n = 6) at +80 mV], whereas the high conductance state had similar values at both voltages (∼2.5 pA). Similar results were obtained when the E340N channel was activated by cAMP. However, from single-channel dose–response curves (data not shown, see Table II), it was found that the maximal open probability of the low conductance state for cAMP at −80 mV was 0.88 ± 0.02 (n = 2), lower than that for cGMP, which was 0.96 ± 0.01 (n = 3).

Therefore, the E340N mutation modifies the gating

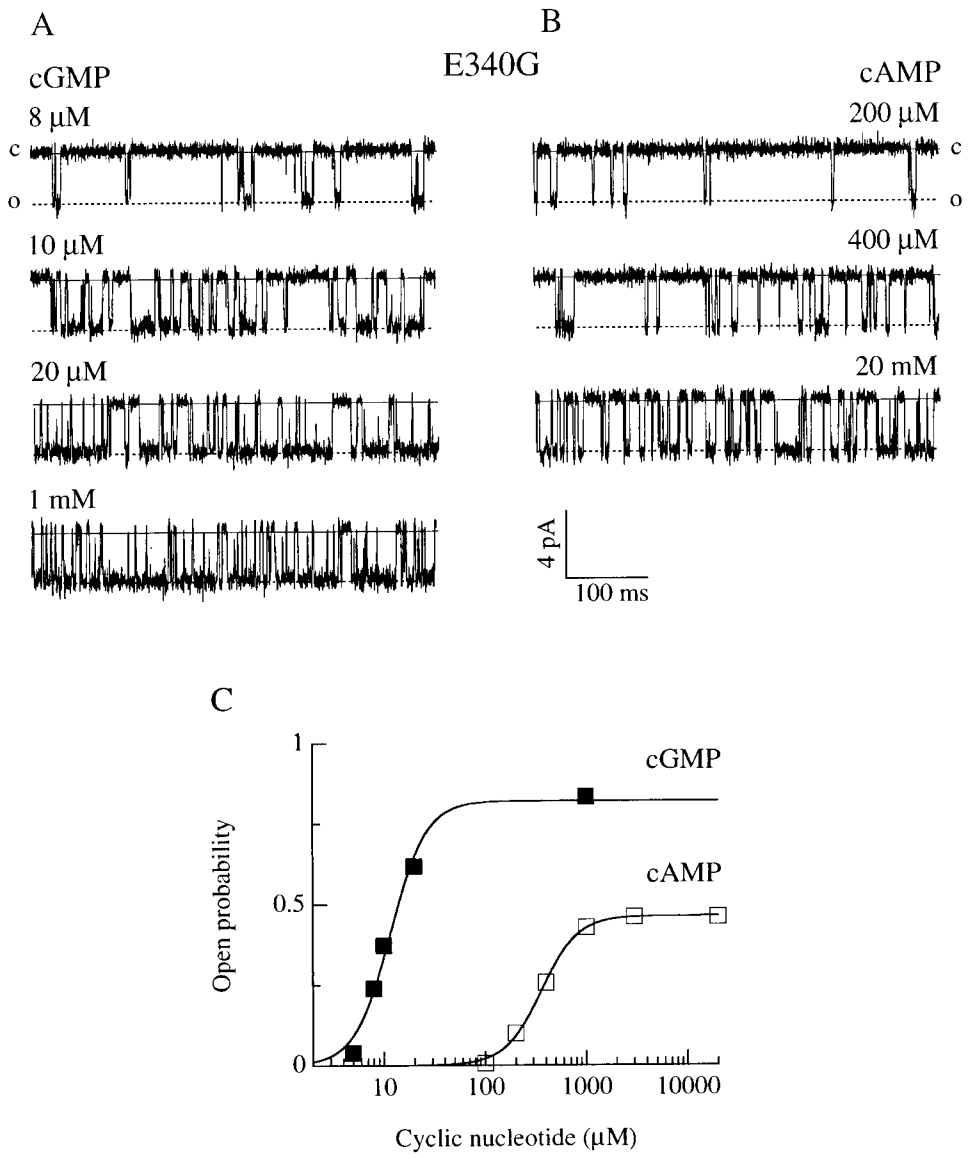

Figure 2. Single-channel dose–response relation for the E340G mutant. Current recordings from a membrane patch containing one E340G channel activated at −80 mV by various concentrations of cGMP (A) or cAMP (B). The continuous lines indicate the closed channel level and the dotted lines indicate the open level. (C) Dose–response relations were plotted as the open probability versus cyclic nucleotide concentration from the patch shown in A and B. Continuous curves were the best fit of the Hill equation (Eq. 2) to the data with the following values: $P_{max,cG} = 0.82$, $K_{1/2,cG} = 11.6$ μM, $n_{cG} = 2.4$, $P_{max,cA} = 0.46$, $K_{1/2,cA} = 360$ μM, $n_{cA} = 2.4$.

properties of the channel by introducing a new conductance state and by reducing the efficacy of activation by cyclic nucleotides more so for cAMP than cGMP.

Voltage Dependence of Permeation Properties

To investigate whether changes in the voltage dependence of the macroscopic currents recorded from various mutants (Fig. 1 A) were due to effects of voltage on the permeation or on the gating process, the I-V relations of macroscopic and single-channel currents for wild-type and mutant channels were compared in Fig. 4. Macroscopic currents were normalized to their respective values measured at +80 mV, and the values of single-channel and normalized macroscopic currents were averaged from several patches and plotted as a function of voltage. For the mutant E340N, only the single-channel current value of the low conductance state, in which the channel spent most of its time, is shown. Among the different channel types, the amplitude and rectification properties of single-channel current varied; however, they did not depend on which cyclic nucleotide, cAMP or cGMP, activated the channel (data not shown). At −80 mV, the average single-channel current was −3.2 pA in the wild-type, −4.8 pA in the mutated channel E340D, −2.6 pA in the E340G, and −0.5 pA for the low-conductance state in the E340N (see Table II). The mean ratio between the single-channel current at −80 and +80 mV was 1.07 in the wild type, 1.26 in the mutated channel E340D, 0.72 in the E340G, and 0.5 for the low conductance state in the E340N.

The superimposition of the single-channel I-V curve with the macroscopic I-V curve for the various channel types indicates that the changes in the rectification properties in different mutants are mainly caused by

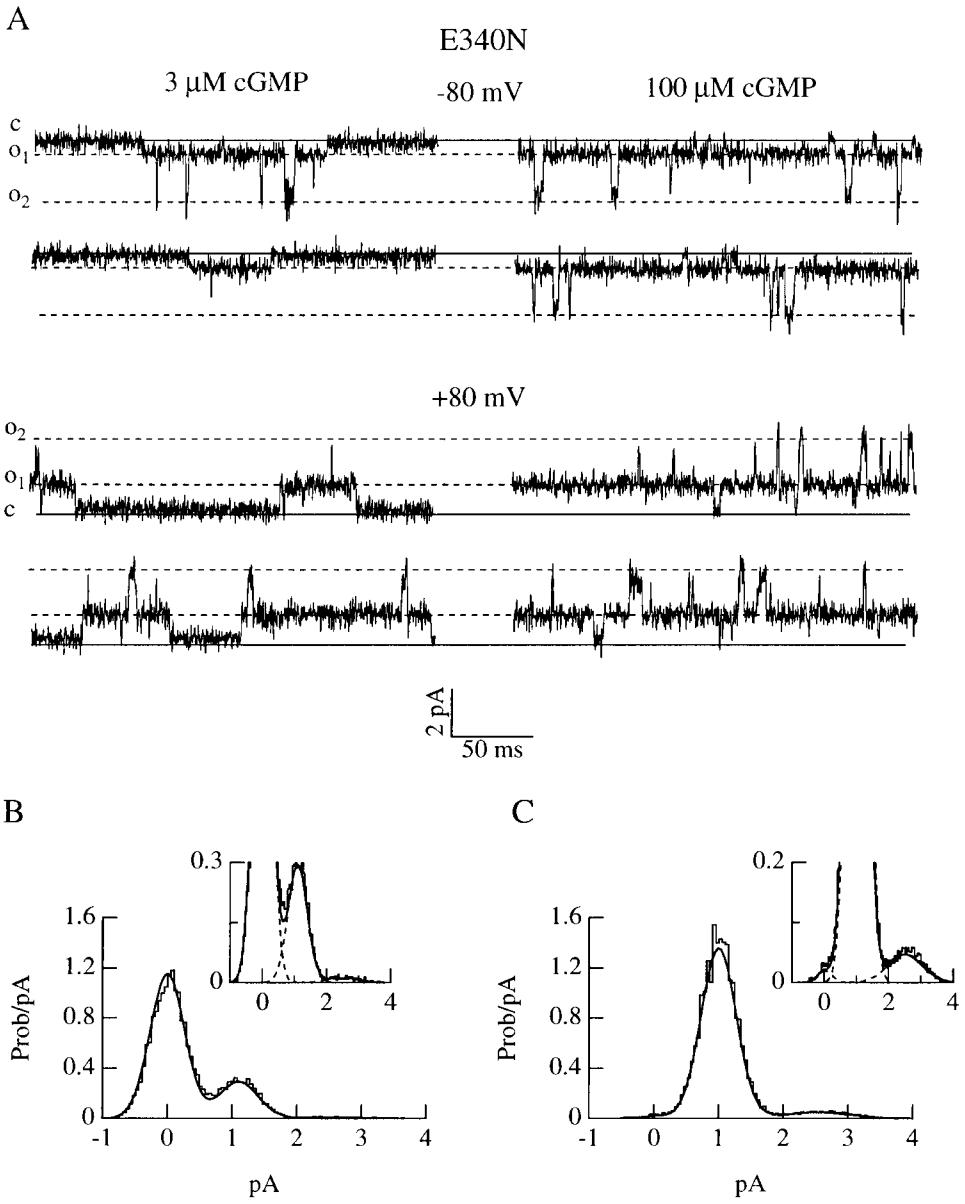

Figure 3. Single-channel voltage and concentration dependence of E340N mutant. (A) Current recordings from a membrane patch containing one E340N channel activated by 3 or 100 μM cGMP at −80 or +80 mV. The continuous lines indicate the closed channel level and the dotted lines indicate two conductance open levels. Amplitude histograms at +80 mV for 3 μM (B) or 100 μM (C) cGMP were fitted as the sum of three Gaussians and shown enlarged in the insets. Histograms were fitted with the following parameters. For 3 μM cGMP: P_{closed} = 0.765, $P_{o,low}$ = 0.22, i_{low} = 1.1 pA, $P_{o,high}$ = 0.015, i_{high} = 2.5 pA; for 100 μM cGMP: P_{closed} = 0.01, $P_{o,low}$ = 0.925, i_{low} = 1 pA, $P_{o,high}$ = 0.065, i_{high} = 2.5 pA.

changes in the voltage dependence of the permeation process, rather than by changes in gating (see also Table II for values of P_{max} at positive and negative voltages).

Gating Model for Channel Activation

The single-channel dose responses of wild-type and mutant channels were plotted in Fig. 5, along with the best fit obtained by Eq. 3. In the presence of cGMP, K_d had similar values: 29 ± 10 μM (n = 3) wild-type and 31 ± 15 μM (n = 3) for E340D, and 24 ± 12 μM (n = 4) for E340G. On the other hand, L varied from 334 ± 82 for the wild-type to 66 ± 15 for E340D and 5.2 ± 1.3 for E340G mutation. In the presence of cAMP, K_d also had similar values: 333 ± 96 μM (n = 3) for wild-type and 558 ± 120 μM (n = 3) for E340D and 479 ± 241 μM (n = 4) for E340G, though these values differ from those obtained for cGMP. L for cAMP varied from 70 ± 22 for the wild type to 12 ± 7 for E340D and 0.6 ± 0.3 for E340G mutant channels.

Therefore, mutant channels have K_d values similar to those estimated for the wild-type channel, but are characterized by very different values of the gating constant L, which determines the value for the maximal open probability. Two major conclusions can be drawn from these results. First, mutations at position 340 do not affect the "effective" dissociation constant (K_d) for cAMP and cGMP. Second, mutations at position 340 modify the opening efficiency of the fully liganded channel. Thus, changes in the value of $K_{1/2}$ in the various mutants originate from changes of L.

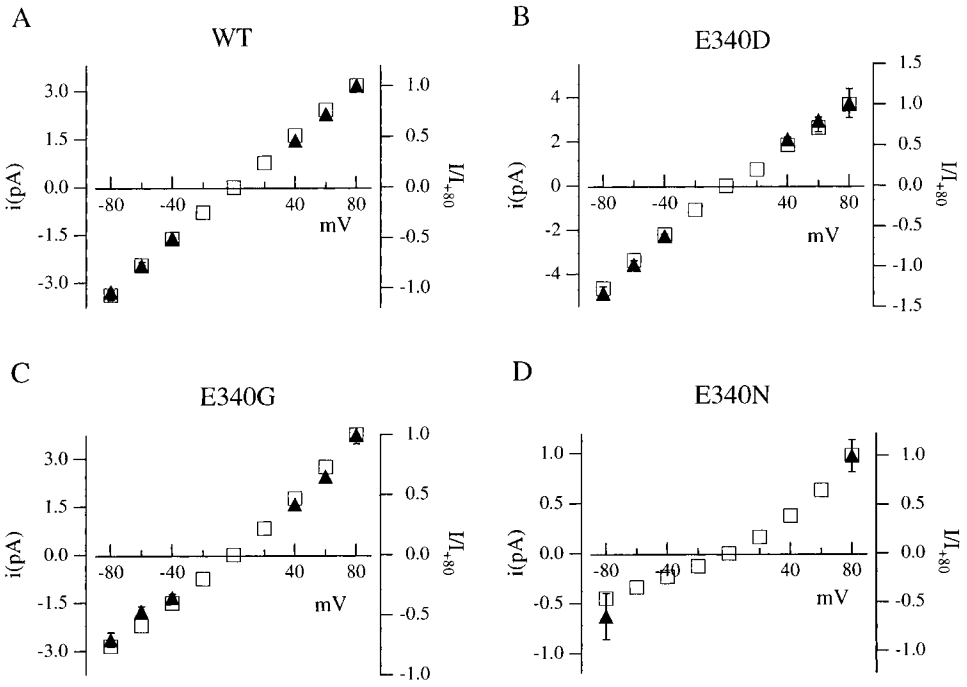

Figure 4. Comparison of normalized I-V relations from macroscopic and single-channel currents for wild-type and mutant channels. Macroscopic currents were measured at saturating cGMP in a voltage range from −80 to + 80 mV and normalized to unity at +80 mV. Average values of normalized macroscopic currents (□) and of single-channel amplitudes (▲) were plotted versus applied voltage. Each point is the average from at least four patches. Bars indicate standard deviation. Error bars smaller than the size of the symbols were not plotted.

Divalent Cation Blockage

It is well known from previous work on the α subunit of the bovine retinal rod CNG channel that E363 controls channel blockage by extracellular divalent cations. We investigated here the role on such blockage of the residue E340 at the corresponding position in the olfactory CNG channel.

First, we measured the macroscopic dose–response relations for currents activated by cAMP or cGMP in inside-out patches from wild-type, E340G, and E340N channels in the presence of 1 mM Ca^{2+} in the patch pipette. The presence of 1 mM external Ca^{2+} did not significantly affect $K_{1/2}$ for either cyclic nucleotide (data not shown), indicating that external Ca^{2+} does not modify the gating properties of these channels (see also Fig. 7).

The blocking effect of external Ca^{2+} and Mg^{2+} was therefore investigated by measuring the I-V relations of wild-type and mutant CNG channels in the presence of increasing Ca^{2+} or Mg^{2+} concentrations at the extracellular side of outside-out patches.

Fig. 6, A and B, (left) shows the I-V relations for wild-type channels in which increasing concentrations of external Ca^{2+} (A) or Mg^{2+} (B) progressively reduced both the inward and outward currents in a voltage-dependent manner. When glutamate 340 was replaced by a neutral asparagine or glycine residue, blockage by external divalent cations was greatly reduced, and even high concentrations of external Ca^{2+} or Mg^{2+}, 5–10 mM, only partially blocked the current (Fig. 6).

To investigate whether an acidic residue at position 340 was crucial for Ca^{2+} and Mg^{2+} blockage, the charge-conserving substitution E340D was analyzed. Fig. 6 shows that external divalent cations powerfully blocked E340D channels, and that the voltage dependence of the blockage by external Ca^{2+} differed from that observed in wild-type channels. Indeed (see also Table III), the blocking effect at positive voltages was

TABLE II

Single-Channel Properties of Wild-Type and Mutant CNG Channels

	P_{max} (−80 mV)				P_{max} (+80 mV)				*i*, pA			
	cAMP		cGMP		cAMP		cGMP		−80 mV		+80 mV	
Wild Type	0.985 ± 0.004	5	0.996 ± 0.001	3	0.984 ± 0.002	2	0.993 ± 0.004	2	−3.2 ± 0.2	17	3.0 ± 0.1	11
E340D	0.958 ± 0.029	4	0.987 ± 0.007	4	0.978 ± 0.009	4	0.985 ± 0.007	2	−4.8 ± 0.2	4	3.8 ± 0.6	4
E340G	0.27 ± 0.12	9	0.79 ± 0.06	9	0.23 ± 0.08	5	0.77 ± 0.08	5	−2.6 ± 0.2	11	3.6 ± 0.3	13
E340N*	0.88 ± 0.02	2	0.96 ± 0.01	3	ND		0.87 ± 0.02	2	−0.5 ± 0.1	5	1.0 ± 0.2	6
E340N‡	0.03 ± 0.01	2	0.04 ± 0.01	3	ND		0.10 ± 0.07	2	−1.8 ± 0.1	4	1.6 ± 0.1	4

P_{max} values are obtained by fitting the experimental data with Eq. 2. All values are means ± SD, with the number of experiments given. *Low level of current; ‡high level of current determined with respect to low level.

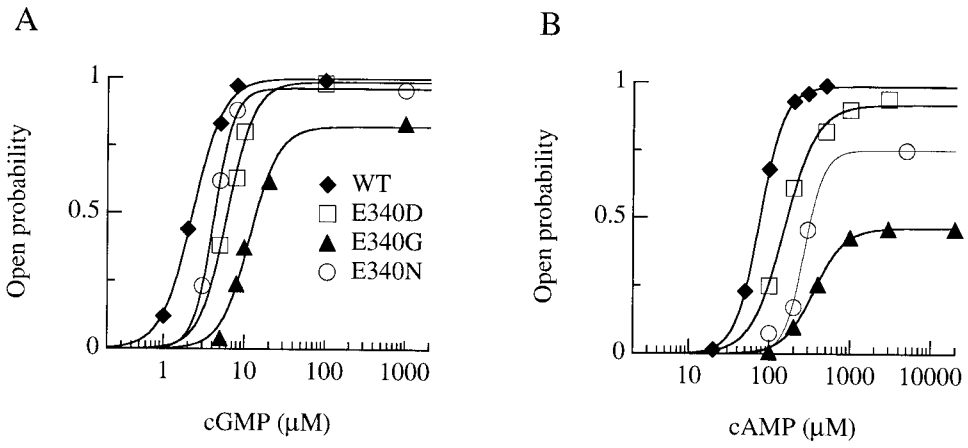

Figure 5. Single-channel dose–response relations for wild-type, E340D, E340N, and E340G channels. Continuous curves show fits of Eq. 3 to the dose–response relations using the following parameters. Wild-type: L_{cG} = 334, $K_{d,cG}$ = 29 μM, n_{cG} = 2.3, L_{cA} = 70, $K_{d,cA}$ = 333 μM, n_{cA} = 2.9; E340D: L_{cG} = 66, $K_{d,cG}$ = 31 μM, n_{cG} = 2.6, L_{cA} = 12, $K_{d,cA}$ = 558 μM, n_{cA} = 3; E340G: L_{cG} = 4.6, $K_{d,cG}$ = 24 μM, n_{cG} = 2.4, L_{cA} = 0.9, $K_{d,cA}$ = 472 μM, n_{cA} = 2.3; E340N: L_{cG} = 10, $K_{d,cG}$ = 24 μM, n_{cG} = 3.5, L_{cA} = 3, $K_{d,cA}$ = 400 μM, n_{cA} = 3.5.

more pronounced in the E340D mutant than in wild-type channels (see discussion).

The concentration dependence of extracellular Ca^{2+} and Mg^{2+} blockage is better illustrated in Fig. 6, C–F. Current values from the experiments shown in Fig. 6, A and B, measured at +80 or −80 mV in the presence of various concentrations of Ca^{2+} or Mg^{2+} were normalized to the current in the absence of divalent cations and plotted versus divalent cation concentration. For external divalent cation blockage at various voltages, K_i was calculated from the best fit of Eq. 4 to the data (see Table III). At −80 mV for Ca^{2+}, K_i was found to increase from a similar average value of 47 ± 21 μM (n = 6) for wild-type and 47 ± 7 μM (n = 6) for E340D, to 6.3 ± 2.5 mM (n = 6) for E340G and 6.5 ± 4.0 mM (n = 4) for E340N mutant channels. At −80 mV for Mg^{2+}, K_i increased from an average value of 70 ± 34 μM (n = 11) for wild-type and 53 ± 17 μM (n = 4) for E340D, to 1.1 ± 0.3 mM (n = 7) for E340G and 17.0 ± 7.2 mM (n = 4) for E340N mutant channels.

The blockage by external divalent cations was also found to be relieved in the E340Q mutant channels (data not shown), with average values reported in Table III. Hill coefficients for wild type and E340D were always close to one, indicating that one divalent cation is likely sufficient to block the pore in these channels. A 1,000-fold higher external divalent concentration was necessary to block 50% of the current in mutant channels with a neutral residue in position 340, and Hill coefficients were below unity.

The blockage by internal Ca^{2+} of wild-type and mutant channels was also investigated. Macroscopic currents in inside-out patches were activated by 1 mM cGMP in the presence of various Ca^{2+} concentrations at the cytoplasmic side of the patch (data not shown), and the average K_i for internal Ca^{2+} blockage at +80 mV was found to be 1.0 ± 0.7 mM (n = 5) for wild-type and 1.5 ± 0.4 mM (n = 4) for E340G mutant channels. Similar results were also found for the E340N mutation. Therefore, charge neutralization of E340 does not significantly modify the blockage by intracellular Ca^{2+} of the olfactory CNG channel.

These results show that the presence of an acidic residue at position 340 of the bovine olfactory channel is an important determinant of blockage by external divalent cations.

Single-Channel Analysis of External Ca^{2+} Blockage

To investigate whether external divalent cation blockage on macroscopic current is due to a change in permeation and/or gating properties of the olfactory CNG channel, single-channel properties were examined. Fig. 7 A shows recordings from a patch in the outside-out configuration containing wild-type channels activated by 5 μM cGMP at −80 mV. At saturating cGMP concentrations, wild-type channels are open most of the time, making it difficult to estimate the single-channel amplitude reliably, so a lower concentration of cGMP was used for estimating the single-channel amplitude. The addition of 50 μM external Ca^{2+} caused a partial blockage of the single-channel current and in the presence of 1 mM Ca^{2+}, no current was detected at −80 mV.

When the same experiments were repeated with a patch containing a single E340G mutant channel (Fig. 7 B), activated by 1 mM cGMP, the single-channel amplitude was only slightly reduced in the presence of 1 or even 10 mM external Ca^{2+}.

Single-channel currents from the patches shown in Fig. 7, A and B, in the presence of increasing concentrations of extracellular Ca^{2+}, were estimated from amplitude histograms. The obtained values were normalized to the single-channel current measured in the absence of divalent cations and plotted as a function of Ca^{2+} concentration at +80 and −80 mV (see Fig. 7, C and D). The best fit of Eq. 4 to the data (continuous lines) gave a value of K_i for Ca^{2+} at +80 mV of 250 μM for wild-type and 32 mM for E340G, while at −80 mV, K_i for Ca^{2+} was 31 μM for wild-type and 8.8 mM for

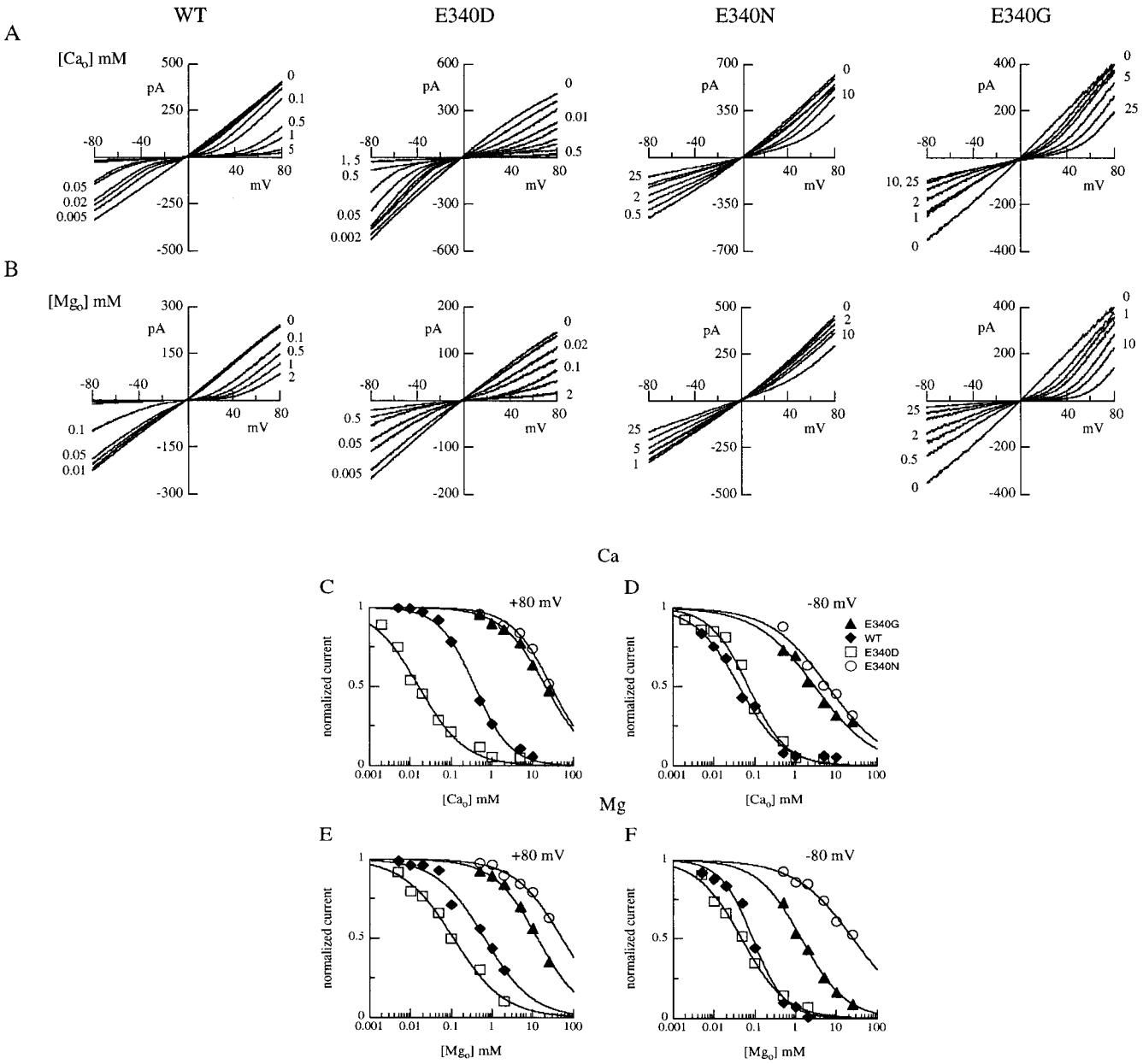

Figure 6. External Ca^{2+} and Mg^{2+} blockage in wild-type and mutant channels. cGMP-gated currents were measured in outside-out patches in the presence of the indicated concentrations of Ca^{2+} (A) or Mg^{2+} (B) in the extracellular solution. Currents were activated by 100 μM cGMP in the patch pipette. Voltage ramps were from −80 to +80 mV. Currents from the experiments shown in A and B in the presence of various Ca^{2+} or Mg^{2+} concentrations were measured at +80 or −80 mV, normalized to the current measured in the absence of divalent cations at the same voltage and plotted as a function of external Ca^{2+} (C–D) or Mg^{2+} (E–F) concentrations. Continuous lines were the best fit of Eq. 4 to the data with the following values. (C) At +80 mV, wild type (◆): $K_{i,Ca}$ = 380 μM, n = 1; E340D (□): $K_{i,Ca}$ = 16 μM, n = 1; E340G (▲): $K_{i,Ca}$ = 21 mM, n = 0.8; E340N (○): $K_{i,Ca}$ = 28 mM, n = 0.9. (D) At −80 mV, wild type (◆): $K_{i,Ca}$ = 42 μM, n = 0.8; E340D (□): $K_{i,Ca}$ = 70 μM, n = 0.9; E340G (▲): $K_{i,Ca}$ = 3 mM, n = 0.6; E340N (○): $K_{i,Ca}$ = 6.3 mM, n = 0.6. (E) At +80 mV, wild type (◆): $K_{i,Mg}$ = 650 μM, n = 0.7; E340D (□): $K_{i,Mg}$ = 112 μM, n = 0.7; E340G (▲): $K_{i,Mg}$ = 13 mM, n = 0.8; E340N (○): $K_{i,Mg}$ = 51 mM, n = 0.7. (F) At −80 mV, wild type (◆): $K_{i,Mg}$ = 90 μM, n = 1.1; E340D (□): $K_{i,Mg}$ = 48 μM, n = 0.8; E340G (▲): $K_{i,Mg}$ = 1.4 mM, n = 0.8; E340N (○): $K_{i,Mg}$ = 26 mM, n = 0.6.

E340G. Similar results were obtained in two other patches for each channel type.

A comparison between these results on single-channel current and those on macroscopic currents (Table III) shows that K_i and n values are in good agreement, indicating that external Ca^{2+} blockage diminishes the single-channel amplitude, affecting permeation rather than gating.

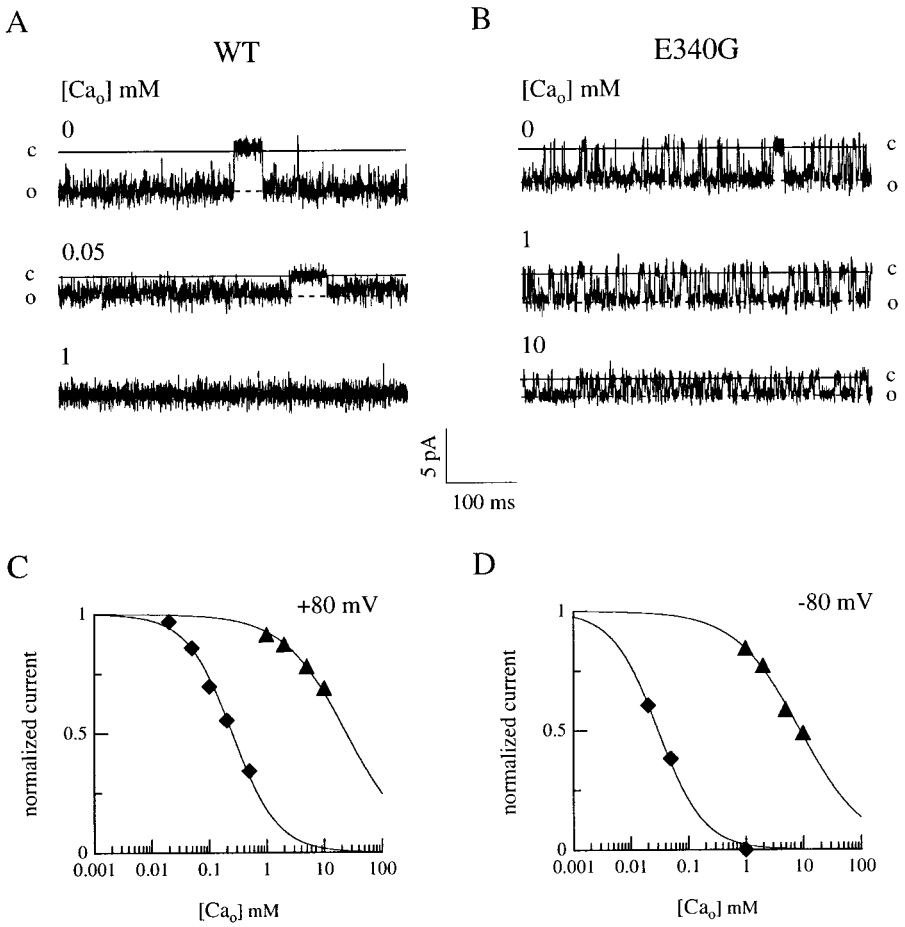

Figure 7. External Ca^{2+} blockage on single-channel current for wild-type and E340G mutant channels. (A and B) Single-channel currents at −80 mV activated by cGMP in outside-out patches in the presence of the indicated concentrations of external Ca^{2+}. The cGMP concentration was 5 μM for wild-type (A) and 1mM for E340G (B) mutant channels. (C and D) Currents from each patch were determined from amplitude histograms in the presence of various Ca^{2+} concentrations at +80 or −80 mV, normalized to the current measured at the same voltage in the absence of divalent cations, and plotted as a function of external Ca^{2+} concentrations (C and D). Continuous lines were the best fit of Eq. 1 to the data with the following values. At +80 mV, (C) wild type (◆): $K_{i,Ca}$ = 250 μM, n = 1; E340G (▲): $K_{i,Ca}$ = 32 mM, n = 0.7. At −80 mV, (D) wild type (◆): $K_{i,Ca}$ = 31 μM, n = 1.1; E340G (▲): $K_{i,Ca}$ = 8.8 mM, n = 0.8.

Divalent Cation Permeation

The permeation of divalent cations was investigated in outside-out patches by substituting external NaCl (110 mM) with equiosmolar concentrations (73.3 mM) of $CaCl_2$ or $MgCl_2$. Channels were activated by 1 mM cGMP in the patch pipette and voltage steps of 150-ms duration from a holding potential of 0 mV were given from −80 to +80 mV in 20-mV steps. Fig. 8, A and B, shows recordings from wild-type and E340G mutants, respectively. I-V relations were plotted in Fig. 8, C and D.

From these experiments, the ratio between the current carried by external Ca^{2+} and Na^+ ions, I_{Ca}/I_{Na}, at −80 mV was calculated. For wild-type channels, the average value of I_{Ca}/I_{Na} at −80 mV was 0.049 ± 0.004 (n = 4) and increased to 0.16 ± 0.03 (n = 6) for E340G mutant channels. The average reversal potential, V_{rev},

TABLE III

Inhibition Constants from Macroscopic Currents from Wild-Type and Mutant CNG Channels

	Ca^{2+}								Mg^{2+}							
	K_i, μM				n				K_i, μM				n			
	−80 mV		+80 mV		−80 mV		+80 mV		−80 mV		+80 mV		−80 mV		+80 mV	
Wild Type	47 ± 21	6	383 ± 145	6	1.3 ± 0.4	6	0.9 ± 0.1	6	70 ± 34	11	920 ± 640	11	1.2 ± 0.2	11	1.0 ± 0.1	11
E340D	47 ± 7	6	18 ± 10	6	1.2 ± 0.5	6	1.3 ± 0.5	6	53 ± 17	4	155 ± 56	4	0.7 ± 0.2	4	0.9 ± 0.2	4
E340G	6300 ± 2500	6	26000 ± 9800	6	0.4 ± 0.1	6	0.6 ± 0.2	6	1100 ± 300	7	9500 ± 3900	7	0.7 ± 0.1	7	0.8 ± 0.2	7
E340N*	6500 ± 4000	4	29000 ± 6000	4	0.6 ± 0.1	4	0.6 ± 0.2	4	17000 ± 7200	4	50000 ± 3600	4	0.6 ± 0.1	7	0.6 ± 0.1	7
E340N‡	2100 ± 600	4	19000 ± 12000	4	0.4 ± 0.2	4	0.5 ± 0.2	4	3400	1	140000	1	0.5	1	0.3	1

Inhibition constants, K_i, and Hill coefficients, n, for the blockage by external Ca^{2+} or Mg^{2+} were obtained from the best fit of Eq. 4 to the data. All values are means ± SD, with the number of experiments given.

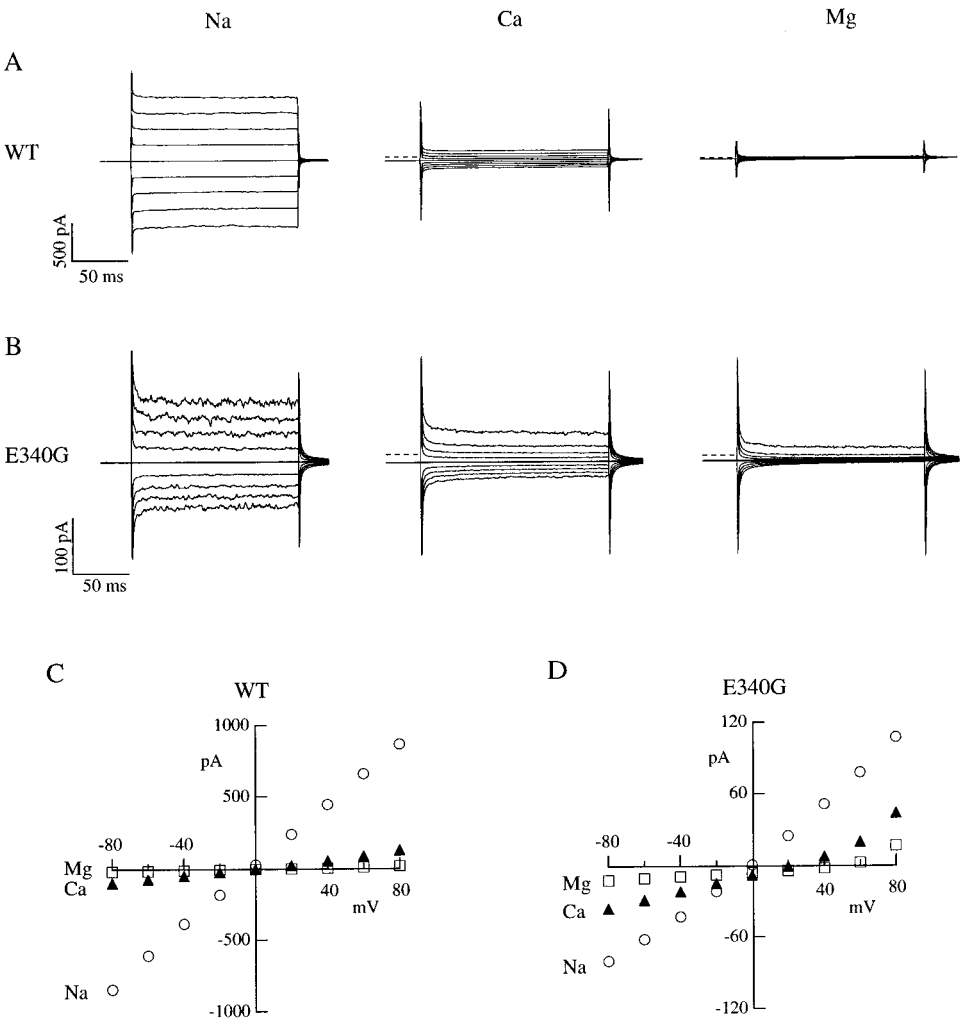

Figure 8. Permeation of external Ca^{2+} and Mg^{2+} in wild-type and E340G mutant channels. Current recordings from individual outside-out patches in bi-ionic conditions. The patch pipette contained 1 mM cGMP and 110 mM NaCl, while the external solution contained either 110 mM NaCl, 73.3 mM $CaCl_2$, or 73.3 mM $MgCl_2$, as indicated in the figure. Voltage was changed in 20-mV steps from −80 to +80 mV from a holding potential of 0 mV. The dashed lines indicate the zero-current level. Raw data are illustrated without leak subtraction. Capacitance artifacts were not subtracted. Current–voltage relations are plotted in C and D for wild-type and E340G, respectively. Symbols indicate the bi-ionic conditions: symmetrical NaCl (○), internal NaCl and external $CaCl_2$ (▲), and internal NaCl and external $MgCl_2$ (□).

under bi-ionic conditions (internal Na and external divalent cations) was 25 ± 6 mV (n = 8) for Ca^{2+} and 45 ± 7 mV (n = 5) for Mg^{2+} for wild-type channels. For E340G mutant channels, V_{rev} was 24 ± 5 mV (n = 5) for Ca^{2+} and 45 ± 15 mV (n = 4) for Mg^{2+}.

These results show that reversal potentials and therefore permeability ratios, were not affected by the E340G mutation. However, the E340G mutation caused an increase of the inward Ca^{2+} current relatively to the Na^+ current.

DISCUSSION

The results presented in this paper demonstrate that the residue at position 340 of the bovine olfactory CNG channel affects permeation and gating properties in the absence of divalent cations and controls the efficacy of blockage by external Ca^{2+} and Mg^{2+} ions. Moreover, our findings highlight similarities and differences with the role played by the corresponding residue 363 of the bovine rod CNG channel.

Gating by cAMP and cGMP

It is well established that cGMP and cAMP elicit similar maximal responses in wild-type olfactory channels, whereas $K_{1/2}$ for cGMP is several-fold lower than that for cAMP. All mutant channels presented in this study had higher $K_{1/2}$ values compared with wild-type channels, and showed a decrease of the maximal current activated by cAMP with respect to cGMP, especially in the E340G mutant. The explanation of these results is not obvious: the decrease in cAMP maximal current could derive either from a reduced single-channel amplitude or from different gating properties of CNG channels when activated by cAMP or cGMP. Moreover, the shift in $K_{1/2}$ could originate from a modification in the binding reactions for cyclic nucleotides (i.e., K_d) or the subsequent allosteric rearrangement leading to channel opening (i.e., L) or from both effects.

Single-channel analysis allowed us to distinguish between these possible explanations. In all tested mutants, the single-channel conductance activated by cAMP and

cGMP was the same, but open probabilities were different: in the E340G mutant P_{max} did not exceed 50% of that observed with cGMP. Moreover, analysis of the data by using an allosteric model similar to that used by Liu et al. (1994) revealed that the substitutions at position 340 leave the effective affinity of the binding steps almost unaffected for a given cyclic nucleotide, but lower the equilibrium gating constant L. Therefore, differences in activation can be explained by assuming that mutants open less easily than wild-type channels without significant changes in the binding of cyclic nucleotides. These results show that the pore is involved in the allosteric conformational change after ligand binding.

Permeation

We found that mutation of E340 caused a modification in the I-V relations. The analysis of single-channel activity (Table II) showed that the rectification of the I-V curves is primarily determined by the voltage dependence of ion permeation rather than of the gating process. This result differs from what was previously measured in retinal rod. Indeed, Root and MacKinnon (1993) showed that the rectification of single-channel currents induced by mutations of E363 is smaller than that of macroscopic currents, implying that the difference must be accounted for by an effect of the mutations on voltage dependence of channel gating.

Two conductance levels were observed in the E340N mutant. Although it was outside the scope of our study to develop a kinetic model explaining these multiple conductance levels, this result further shows that the bovine olfactory CNG channel has single-channel properties different from those of the catfish olfactory CNG channel. Indeed, the CNG channel from catfish has multiple conductance states (Goulding et al., 1992) that have been ascribed to protonation of the glutamate residue (Root and MacKinnon, 1994). One of the key experiments aimed at demonstrating that these subconductance states arise from proton binding in the pore was to show that they are not present when glutamate was replaced with the neutral glycine (Root and MacKinnon, 1994). We found here that, although subconductance states are not evident in the wild-type bovine olfactory CNG channel, multiple conductance states are present when glutamate was replaced with the neutral asparagine, E340N, suggesting that proton block of the 340 residue is not responsible for subconductance states.

These results show that channels from different species could have some specific properties that are not necessarily shared by the majority of CNG channels, despite belonging to the same class.

Divalent Cation Blockage

Ca^{2+} and Mg^{2+} block the current carried by Na^+ ions through olfactory CNG channels from the extracellular side and to a lesser extent from the intracellular side. The external divalent cation blockage was drastically reduced in mutant channels where E340 was replaced by a neutral amino acid (Table I), while internal divalent blockage was largely unaffected. These findings are in agreement with similar results obtained with mutations at position E363 of the α subunit from bovine retinal rods (Root and MacKinnon, 1993; Eismann et al., 1994; Park and MacKinnon, 1995).

A special case is the E340D mutant. The charge-conserving mutation E340D preserved the external divalent cation blockage, but altered its voltage dependence with a more pronounced effect for Ca^{2+} than for Mg^{2+} (Table III). Indeed, we unexpectedly found that external Ca^{2+} blockage was more effective at positive (K_i = 18 μM at +80 mV) than negative (K_i = 47 μM at −80 mV) voltages. In the E363D mutant from retinal rods (Root and MacKinnon, 1993; Park and MacKinnon, 1995; Seifert et al., 1999), the external divalent cation blockage was also preserved, although the voltage dependence was not dramatically altered as in the olfactory channel.

How can the different voltage dependence between Ca^{2+} and Mg^{2+} blockage in the olfactory E340D channel be explained? A similar result has also been previously observed in the blockage by internal divalent cations in native CNG channels from retinal rods (Colamartino et al., 1991; Zimmerman and Baylor, 1992). The voltage dependence of block by internal Ca^{2+} was opposite that of block by internal Mg^{2+} (see Figure 10, B and C, from Zimmerman and Baylor, 1992): Mg^{2+} in the internal solution caused a strong inward rectification, while Ca^{2+} caused a very pronounced outward rectification. Zimmerman and Baylor (1992) proposed a simple model, based on Eyring rate theory, in which cations permeate and block the channel by combining with a single binding site located in the transmembrane electrical field. They showed that the opposite voltage dependence of blockage by Ca^{2+} and Mg^{2+} arises from their different energy profiles for permeation: for Mg^{2+}, the external barrier is higher than the internal barrier and depolarization favors occupancy of the well by internal Mg^{2+}; for Ca^{2+}, the internal barrier is higher and depolarization disfavors the occupancy of the well by internal Ca^{2+} (see Figure 1 in Zimmerman and Baylor, 1992). A similar model can be used to explain the different voltage dependence of blockage by external Ca^{2+} and Mg^{2+} between the wild-type and E340D mutant channel; i.e., the mutation could differentially alter the external barrier for Ca^{2+} and Mg^{2+}.

From a molecular point of view, these differences could have several origins. Although glutamate and aspartate have the same charge, they have a different length of the amino acid side chains and the protonation of aspartate could be different from that of glutamate. Alternatively,

the binding site may change its location within the transmembrane electrical field, and/or the stereochemical coordination of divalent cations may be altered.

Comparison with Native Channels

The voltage dependence of blockage in α3 homomers and native channels is largely similar in that blockage was more pronounced at negative than at positive potentials. However, the values for K_i were different. The K_i for external Ca^{2+} blockage in native olfactory CNG channels from the frog *Rana esculenta* was found to be 265 μM at −70 mV and ∼2 mM at +80 mV (see Figure 6 B of Dzeja et al., 1999; see also Kleene, 1995), while in α3 homomers we found 47 μM at −80 mV and 383 μM at +80 mV. These different K_i values could originate from the different subunit composition of native channels: indeed, native olfactory CNG channels from the olfactory sensory neurons of the rat are composed by the coassembly of the three different types of subunits α3, α4, and β1b (Bönigk et al. 1999) having a glutamate, an aspartate, and a glycine residue, respectively, at the positions corresponding to E340 of the α3 subunit of bovine olfactory CNG channels. These residues are likely to play the key role in the blockage by external divalent cations, since we have shown that mutation of glutamate at position 340 of the α3 subunit into aspartate or glycine changes the sensitivity to external Ca^{2+} and Mg^{2+} by more than two orders of magnitude.

Recent experiments by Kleene (1999) show that external Ca^{2+} reduces the sensitivity to cAMP of the native olfactory channel with a mechanism different from the effect of cytoplasmic Ca^{2+}. In the presence of 3 mM external Ca^{2+}, $K_{1/2}$ for cAMP increased eightfold. We did not observe this effect in our experiments, using expressed channels composed only of the principal α3 subunit. Hackos and Korenbrot (1999) found that divalent cation selectivity depends on the cGMP concentration in retinal rod recombinant channels composed of α and β subunits, and not on channels formed from α subunits alone. Whether the additional olfactory subunits are responsible for the reduced sensitivity to cAMP induced by external Ca^{2+} in native olfactory channels remains to be determined.

We thank V. Torre, F. Gambale and A. Miri for comments on the manuscript and F. Pittaluga, G. Boido, G. Gaggero, P.G. Gagna, D. Magliozzi, and P. Guastavino for technical assistance. L. Giovanelli checked the English. Special thanks to B. Norcio for many helpful discussions.

This work was supported by European Community contract BIO4-CT96-0593 (U.B. Kaupp and A. Menini) and a grant from the Ministerium für Wissenschaft und Forschung des Landes Nordrhein-Westfalen IVA-10201095 (U.B. Kaupp).

Submitted: 15 May 2000
Revised: 26 June 2000
Accepted: 27 June 2000

REFERENCES

Altenhofen, W., J. Ludwig, E. Eismann, W. Kraus, W. Bönigk, and U.B. Kaupp. 1991. Control of ligand specificity in cyclic nucleotide-gated channels from rod photoreceptors and olfactory epithelium. *Proc. Natl. Acad. Sci. USA.* 88:9868–9872.

Becchetti, A., K. Gamel, and V. Torre. 1999. Cyclic nucleotide–gated channels. Pore topology studied through the accessibility of reporter cysteines. *J. Gen. Physiol.* 114:377–392.

Bönigk, W., J. Bradley, F. Müller, F. Sesti, I. Boekhoff, G.V. Ronnett, U.B. Kaupp and S. Frings. 1999. The native rat olfactory cyclic nucleotide-gated channel is composed of three distinct subunits. *J. Neurosci.* 13:5332–5347.

Bradley, J., J. Li, N. Davidson, H.A. Lester, and K. Zinn. 1994. Heteromeric olfactory cyclic nucleotide-gated channels: a subunit that confers increased sensitivity to cAMP. *Proc. Natl. Acad. Sci. USA.* 91:8890–8894.

Brown, R.L., W.V. Geber, and J.W. Karpen. 1993. Specific labeling and permanent activation of the retinal rod cGMP-activated channel by the photoaffinity analog 8-*p*-azidophenacylthio-cGMP. *Proc. Natl. Acad. Sci. USA.* 90:5369–5373.

Brown, R.L., S.D. Snow, and T.L. Haley. 1998. Movement of gating machinery during the activation of rod cyclic nucleotide-gated channels. *Biophys. J.* 75:825–833.

Bucossi, G., M. Nizzari, and V. Torre. 1997. Single-channel properties of ionic channels gated by cyclic nucleotides. *Biophys. J.* 72: 1165–1181.

Colamartino, G., A. Menini, and V. Torre. 1991. Blockage and permeation of divalent cations through the cyclic GMP-activated channel from tiger salamander retinal rods. *J. Physiol.* 440:189–206.

Dhallan, R.S., K.-W. Yau, K.A. Schrader, and R.R. Reed. 1990. Primary structure and functional expression of a cyclic nucleotide-activated channel from olfactory neurons. *Nature.* 347:184–187.

Dzeja C., V. Hagen., U.B. Kaupp, and S. Frings. 1999. Ca^{2+} permeation in cyclic nucleotide-gated channels. *EMBO (Eur. Mol. Biol. Organ.) J.* 18:131–144.

Eismann, E., F. Muller, S.H. Heinemann and U.B. Kaupp. 1994. A single negative charge within the pore region of a cGMP-gated channel controls rectification, Ca^{2+} blockage, and ionic selectivity. *Proc. Natl. Acad. Sci. USA.* 91:1109–1113.

Fabiato, A. 1988. Computer programs for calculating total from specified free or free from specified total ionic concentrations in aqueous solutions containing multiple metals and ligands. *Methods Enzymol.* 157:378–417.

Finn, J.T., M.E. Grunwald, and K.W. Yau. 1996. Cyclic nucleotide-gated ion channels: an extended family with diverse functions. *Annu. Rev. Physiol.* 58:395–426.

Fodor, A.A., K.D. Black, and W.N. Zagotta. 1997. Tetracaine reports a conformational change in the pore of cyclic nucleotide–gated channels. *J. Gen. Physiol.* 110:591–600.

Frings, S., R. Seifert, M. Godde, and U.B. Kaupp. 1995. Profoundly different calcium permeation and blockage determine the specific function of distinct cyclic nucleotide-gated channels. *Neuron.* 15:169–179.

Gavazzo, P., C. Picco, and A. Menini. 1997. Mechanisms of modulation by internal protons of cyclic nucleotide-gated channels cloned from sensory receptor cells. *Proc. R. Soc. Lond. B Biol. Sci.* 264:1157–1165.

Gordon, S.E., and W.N. Zagotta. 1995. Localization of regions affecting an allosteric transition in cyclic nucleotide-activated channels. *Neuron.* 14:857–864.

Gordon, S.E., M.D. Varnum, and W.N. Zagotta. 1997. Direct interaction between amino- and carboxyl-terminal domains of cyclic nucleotide-gated channels. *Neuron.* 19:431–441.

Goulding, E.H., J. Ngai, R.H. Kramer, S. Colicos, R. Axel., S.A. Siegelbaum, and A. Chess. 1992. Molecular cloning and single channel properties of the cyclic nucleotide-gated channel from catfish olfactory neurons. *Neuron*. 8:45–58.

Goulding, E.H., G.R. Tibbs, and S.A. Siegelbaum. 1994. Molecular mechanism of cyclic-nucleotide-gated channel activation. *Nature.* 372:369–374.

Hackos, D.H., and J.I. Korenbrot. 1999. Divalent cation selectivity is a function of gating in native and recombinant cyclic nucleotide–gated ion channels from retinal photoreceptors. *J. Gen. Physiol.* 113:799–817.

Herlitze, S., and M. Koenen. 1990. A general and rapid mutagenesis method using polymerase chain reaction. *Gene.* 91:143–147.

Kaupp, U.B., T. Niidome, T. Tanabe, S. Terada, W. Bönigk, W. Stühmer, N.J. Cook, K. Kangawa, H. Matsuo, T. Hirose, et al. 1989. Primary structure and functional expression from complementary DNA of the rod photoreceptor cyclic GMP-gated channel. *Nature*. 342:762–766.

Kaupp, U.B. 1995. Family of cyclic nucleotide gated ion channels. *Curr. Opin. Neurobiol.* 5:434–442.

Kleene, S.J. 1995. Block by external calcium and magnesium of the cyclic nucleotide-activated current in olfactory cilia. *Neuroscience.* 66:1001–1008.

Kleene, S.J. 1999. Both external and internal calcium reduce the sensitivity of the olfactory cyclic nucleotide-gated channel to cAMP. *J. Neurophysiol.* 81:2675–2682.

Liman, E.R., and L.B. Buck. 1994. A second subunit of the olfactory cyclic nucleotide-gated channel confers high sensitivity to cAMP. *Neuron*. 13:611–621.

Liu, M., T.Y. Chen, B.Ahamed, J. Li, and K.W. Yau. 1994. Calcium-calmodulin modulation of the olfactory cyclic nucleotide-gated cation channel. *Science.* 266:1348–1354.

Melton, D.A., P.A. Krieg, M.R. Rebagliati, Maniatis, T.K. Zinn, and M.R. Green. 1984. Efficient *in vitro* synthesis of biologically active RNA and RNA hybridization probes from plasmids containing a bacteriophage SP6 promoter. *Nucleic Acid Res.* 12:7035–7056.

Menini, A., and B.J. Nunn. 1990. The effect of pH on the cyclic GMP-activated conductance in retinal rods. *In* Sensory Transduction. A. Borsellino, L. Cervetto, and V. Torre, editors. Plenum Publishing Corp., New York, NY. 175–181.

Menini, A. 1995. Cyclic nucleotide-gated channels in visual and olfactory transduction. *Biophys. Chem.* 55:185–196.

Menini, A. 1999. Calcium signalling and regulation in olfactory neurons. *Curr. Opin. Neurobiol.* 9:419–426.

Nakamura, T., and G.H. Gold. 1987. A cyclic nucleotide-gated conductance in olfactory receptor cilia. *Nature.* 325:442–444.

Paoletti, P., E.C. Young, and S.A. Siegelbaum. 1999. C-linker of cyclic nucleotide-gated channels controls coupling of ligand binding to channel gating. *J. Gen. Physiol.* 113:17–33.

Park, C.S., and R. MacKinnon. 1995. Divalent cation selectivity in a cyclic nucleotide-gated ion channel. *Biochemistry.* 34:13328–13333.

Perry, R.J., and P.A. McNaughton 1991. Response properties of cones from the retina of the tiger salamander. *J. Physiol.* 433:561–587.

Picones, A., and J.I. Korenbrot. 1995. Permeability and interaction of Ca with cGMP-gated ion channels differ in retinal rod and cone photoreceptors. *Biophys. J.* 69:120–127.

Root, M.J., and R. MacKinnon. 1993. Identification of an external divalent cation-binding site in the pore of a cGMP-activated channel. *Neuron*. 11:459–466.

Root, M.J., and R. MacKinnon. 1994. Two identical noninteracting sites in an ion channel revealed by proton transfer. *Science.* 265: 1852–1856.

Sanger, F., S. Nicklen, and A.R. Coulson. 1977. DNA sequencing with chain-terminating inhibitors. *Proc. Natl. Acad. Sci. USA.* 74: 5463–5467.

Sautter, A., X. Zong, F. Hofmann, and M. Biel. 1998. An isoform of the rod photoreceptor cyclic nucleotide-gated channel beta subunit expressed in olfactory neurons. *Proc. Natl. Acad. Sci. USA.* 95: 4696–4701.

Scott, S.P., and J.C. Tanaka. 1998. Three residues predicted by molecular modeling to interact with the purine moiety alter ligand binding and channel gating in cyclic nucleotide-gated channels. *Biochemistry.* 37:17239–17252.

Seifert, R., E. Eismann, J. Ludwig, A. Baumann, and U.B. Kaupp. 1999. Molecular determinants of a Ca^{2+}-binding site in the pore of cyclic nucleotide-gated channels: S5/S6 segments control affinity of intrapore glutamates. *EMBO (Eur. Mol. Biol. Organ.) J.* 18: 119–130.

Sun, Z.-P., H.A. Myles, E.H. Goulding A. Karlin, and S.A. Siegelbaum. 1996. Exposure of residues in cyclic nucleotide-gated channel pore: P region structure and function in gating. *Neuron*. 16:141–149.

Sunderman, E.R., and W.N. Zagotta. 1999a. Mechanism of allosteric modulation of rod cyclic nucleotide-gated channels. *J. Gen. Physiol.* 113:601–619.

Sunderman, E.R., and W.N. Zagotta. 1999b. Sequence of events underlying the allosteric transition of rod cyclic nucleotide–gated channels. *J. Gen. Physiol.* 113:621–640.

Tibbs, G.R., E.H. Goulding, and S.A. Siegelbaum. 1997. Allosteric activation and tuning of ligand efficacy in cyclic nucleotide-gated channels. *Nature.* 386:612–615.

Varnum, M.D., K.D. Black, and W.N. Zagotta. 1995. Molecular mechanism for ligand discrimination of cyclic nucleotide-gated channels. *Neuron*. 15:619–625.

Varnum, M.D., and W.N. Zagotta. 1997. Interdomain interactions underlying activation of cyclic nucleotide gated channels. *Science.* 278:110–113.

Zagotta, W.N., and S.A. Siegelbaum. 1996. Structure and function of cyclic nucleotide-gated channels. *Annu. Rev. Neurosci.* 19:235–263.

Zimmerman, A.L. 1995. Cyclic nucleotide-gated channels. *Curr. Opin. Neurobiol.* 5:296–303.

Zimmerman, A., and D.A. Baylor. 1992. Cation interactions within the cyclic GMP-activated channel of retinal rods from the tiger salamander. *J. Physiol.* 449:759–783.

Zimmerman, A., J.W. Karpen, and D.A. Baylor. 1988. Hindered diffusion in excised membrane patches from retinal rods outer segments. *Biophys. J.* 54:351–355.

Zong, X., H. Zucker, F. Hofmann, and M. Biel. 1998. Three amino acids in the C-linker are major determinants of gating in cyclic nucleotide-gated channel. *EMBO (Eur. Mol. Biol. Organ.) J.* 17: 353–362.